

# Boussinesq-type equations with improved nonlinear performance

Andrew B. Kennedy\*, James T. Kirby, Qin Chen, Robert A. Dalrymple

*Center for Applied Coastal Research, University of Delaware, Newark, DE 19716, USA.*

Received 19 November 1999; accepted 27 June 2000

---

## Abstract

In this paper, we derive and test a set of extended Boussinesq equations with improved nonlinear performance. To do this, the concept of a reference elevation is further generalised to include a time-varying component that moves with the instantaneous free surface. It is found that, when compared to Stokes-type expansions of the second harmonic and fully nonlinear potential flow computations, both theoretical and practical nonlinear performance can be considerably improved. Finally, a special case of the extended equations is found to have properties which are invariant with respect to the still water datum. © 2001 Elsevier Science B.V. All rights reserved.

*Keywords:* Boussinesq equations; Water waves; Numerical methods; Stokes-type expansions

---

## 1. Introduction

Over the last decade, the usefulness of variable depth Boussinesq-type equations has increased greatly. From their beginnings [1], where they were accurate only for mildly dispersive, mildly nonlinear water waves, the practical range of applicability has been repeatedly increased so that Boussinesq equations of various types are now commonly used to model linear wave propagation up to or beyond the nominal deep water limit of  $kh = \pi$ , and for strongly nonlinear waves in shallow depths.

These improvements may be broadly divided into three main categories. Those in the first category manipulate terms that are formally zero to the order of approximation to obtain dispersive (and sometimes shoaling) properties that are considerably improved. Although certain properties of the equations take on higher order characteristics, the overall order remains the same. This was the first approach used and is typified by the papers of Madsen et al. [2], Madsen and Sørensen [3], and Nwogu [4]. Madsen and colleagues applied differential operators to leading order terms in order to obtain additional “enhancement” terms that had no physical significance, but did not affect the formal validity of the equations. The choice of several resulting constants was made by considering linear dispersion and shoaling properties. In contrast, Nwogu rederived the Boussinesq equations in terms of the velocity at an arbitrary elevation,  $z_\alpha$ . The particular choice of  $z_\alpha$  was made by considering linear dispersion. Both of these approaches yielded dispersion relationships that could become Padé [2, 2] approximants to the exact linear relationship, which gave good results from shallow water up to a dimensionless wavenumber of  $kh = 3$ , and represented a large improvement in applicability. Other papers using this approach are [5], Section 4.

---

\* Corresponding author. Tel.: +1-302-831-4171; fax: +1-302-831-1228.  
*E-mail address:* kennedy@coastal.udel.edu (A.B. Kennedy).

Generally, only linear properties have been considered for optimisation [2–4]. ([5], Section 6, did find four discrete sets of Boussinesq equations with identical linear dispersion, but with differing nonlinear behaviour.) In a general sense, optimisation of linear properties has usually led to linear characteristics that were acceptable to some specified dimensionless wavenumber, while error in nonlinear properties increased more rapidly with increasing depth.

The second area of improvement is simply to retain more nonlinear terms which appear in the surface boundary conditions up to the assumed level of dispersion. This work is typified by the “fully-nonlinear” equations of Wei et al. [6], which, along with the paper, shall henceforth be referred to as WKGS. Essentially, these are Nwogu’s equations [4], but retaining all nonlinear dispersive terms that were found at  $O(\mu^2)$ . Significant improvements in nonlinear wave behaviour were found using these additional terms. Other authors [7,8] have studied the nonlinearity required for the proper representation of wave-current interaction. These types of improvements have also found a wide use.

The final general area of improvement is to assume a more complex structure for the underlying fluid flow. Since this allows a better representation of the internal fluid velocity structure, linear and nonlinear accuracy of the resulting Boussinesq equations increases. By increasing the degree of terms kept from  $O(\mu^2)$  to  $O(\mu^4)$ , Gobbi et al. [9] and Madsen and Schäffer [5], Sections 2, 4 and 5, developed consistent, higher order Boussinesq equations. Each of these papers used all three techniques discussed — i.e. manipulation of error terms, retention of nonlinearity, and use of a more complex flow field — to provide very accurate sets of Boussinesq-type equations. However, due to the complexity of the resulting equations, and the more complicated numerical representation required, this approach has not been adopted as widely as the first two.

In this paper, the nonlinearity of Boussinesq equations is consistently manipulated to produce new sets of equations with improved nonlinear behaviour. This is akin to the error manipulation approach previously described, but in a nonlinear sense. To do this, the  $z_\alpha$  parameter used in Nwogu [4] and WKGS is generalised to include a time varying component dependent on water surface elevation. The resulting equations are found to have considerably improved performance when compared to Stokes-type expansions and accurate potential flow solutions.

## 2. Derivation of extended WKGS equations

The new equations may be considered as a superset of the WKGS equations, extending them to consider a reference elevation,  $z_\alpha$ , that varies in time. The derivation will follow very closely that of WKGS, and thus only the portions where the two derivations differ will be shown.

To provide order of magnitude estimates for scaling, it is most convenient to use dimensionless variables. After choosing  $a_0$ ,  $h_0$ , and  $k_0$  as representative wave amplitude, water depth, and wavenumber, (e.g. [10], WKGS), dimensionless variables become

$$\begin{aligned} (x', y') &= k_0(x, y), & z' &= \frac{z}{h_0}, & \eta' &= \frac{\eta}{a_0} \\ t' &= k_0(gh_0)^{1/2}t, & \phi' &= \left[ \frac{a_0}{k_0h_0}(gh_0)^{1/2} \right]^{-1} \phi, & h' &= \frac{h}{h_0} \end{aligned} \quad (1)$$

where  $(x, y)$  are the horizontal coordinates,  $z$  is the vertical coordinate,  $\eta$  is the surface elevation,  $t$  is time,  $\phi$  is the velocity potential,  $g$  is gravitational acceleration, and  $h$  is the still water depth. For clarity, primes will be neglected during the derivation, as all subsequent equations in this section will be in dimensionless variables.

### 2.1. A time-varying $z_\alpha$

From WKGS, and using their notation, the velocity potential expanded about a reference level  $z_\alpha$  is

$$\phi = \phi_\alpha + \mu^2 \left[ (z_\alpha - z) \nabla \cdot (h \nabla \phi_\alpha) + \frac{1}{2} (z_\alpha^2 - z^2) \nabla^2 \phi_\alpha \right] + O(\mu^4) \quad (2)$$

where  $\delta = a_0/h_0$  and  $\mu^2 = (k_0h_0)^2$  are respectively measures of nonlinearity and dispersion. In WKGS, the reference level,  $z_\alpha$ , is assumed to be a function of horizontal spatial dimensions ( $x, y$ ), but not of time. If we assume that  $z_\alpha$  is also a function of time, the temporal derivative of the velocity potential then becomes

$$\phi_t = \phi_{\alpha t} + \mu^2 \left[ (z_\alpha - z) \nabla \cdot (h \nabla \phi_{\alpha t}) + \frac{1}{2} (z_\alpha^2 - z^2) \nabla^2 \phi_\alpha \right] + \mu^2 [z_{\alpha t} \nabla \cdot (h \nabla \phi_\alpha) + z_\alpha z_{\alpha t} \nabla^2 \phi_\alpha] \quad (3)$$

Compared to WKGS, the last set of terms is new, and obviously arises because  $z_\alpha$  varies in time.

From here, the two-equation ( $\eta, \phi_\alpha$ ) model follows simply. The conservation of mass equation remains unchanged from the WKGS two-equation model

$$\eta_t + \nabla \cdot \mathbf{M} = 0 \quad (4)$$

where

$$\mathbf{M} = \int_{-h}^{\delta\eta} \nabla \phi \, dz \quad (5)$$

and thus

$$\begin{aligned} \mathbf{M} = (h + \delta\eta) \left\{ \nabla \phi_\alpha + \mu^2 \nabla \left[ z_\alpha \nabla \cdot (h \nabla \phi_\alpha) + \frac{1}{2} (z_\alpha^2) \nabla^2 \phi_\alpha \right] \right. \\ \left. + \frac{1}{2} (\mu^2) (h - \delta\eta) \nabla [\nabla \cdot (h \nabla \phi_\alpha)] - \frac{1}{6} \mu^2 (h^2 - h\delta\eta + \delta^2 \eta^2) \nabla^2 \nabla \phi_\alpha \right\} \end{aligned} \quad (6)$$

The Bernoulli equation, however, changes to

$$\begin{aligned} \eta + \phi_{\alpha t} + \frac{1}{2} \delta (\nabla \phi_\alpha)^2 + \mu^2 \left\{ (z_\alpha - \delta\eta) \nabla \cdot (h \nabla \phi_{\alpha t}) + \frac{1}{2} [z_\alpha^2 - (\delta\eta)^2] \nabla^2 \phi_{\alpha t} \right\} \\ + \delta \mu^2 A_1 + \delta \mu^2 A_2 + \delta \mu^2 A_3 + \mu^2 A_4 = 0 \end{aligned} \quad (7)$$

where

$$\begin{aligned} A_1 &= \nabla \phi_\alpha \cdot [\nabla z_\alpha \nabla \cdot (h \nabla \phi_\alpha) + (z_\alpha - \delta\eta) \nabla (\nabla \cdot (h \nabla \phi_\alpha))], \\ A_2 &= \frac{1}{2} [\nabla \cdot (h \nabla \phi_\alpha)]^2 + \delta\eta \nabla \cdot (h \nabla \phi_\alpha) \nabla^2 \phi_\alpha + \frac{1}{2} (\delta\eta)^2 (\nabla^2 \phi_\alpha)^2, \\ A_3 &= \nabla \phi_\alpha \cdot \left[ z_\alpha \nabla z_\alpha \nabla^2 \phi_\alpha + \frac{1}{2} (z_\alpha^2 - (\delta\eta)^2) \nabla (\nabla^2 \phi_\alpha) \right], \\ A_4 &= z_{\alpha t} [\nabla \cdot (h \nabla \phi_\alpha) + z_\alpha \nabla^2 \phi_\alpha] \end{aligned} \quad (8)$$

The only term here that is not in WKGS is  $A_4$ .

The two-equation model based on a velocity potential is not desirable for practical purposes as fourth derivative terms arise when Eq. (6) is substituted into Eq. (4). When represented by finite differences, these can be quite susceptible to noise. Thus, in common with WKGS, we will convert to a three equation  $\eta, \mathbf{u}_\alpha$  model, and reduce the order of the highest derivative to three. We will note that, since the original equations were derived from a velocity potential, the three-equation model will strictly be valid only for the condition of zero vertical vorticity. After defining  $\mathbf{u}_\alpha$  as

$$\mathbf{u}_\alpha = \nabla \phi|_{z=z_\alpha} \quad (9)$$

the gradient of the velocity potential becomes

$$\nabla \phi_\alpha = \mathbf{u}_\alpha - \mu^2 [\nabla z_\alpha \nabla \cdot (h \mathbf{u}_\alpha) + z_\alpha \nabla z_\alpha \nabla \cdot \mathbf{u}_\alpha] + O(\mu^4) \quad (10)$$

and thus

$$\nabla \phi_{\alpha t} = \mathbf{u}_{\alpha t} - \mu^2 [\nabla z_\alpha \nabla \cdot (h \mathbf{u}_{\alpha t}) + z_\alpha \nabla z_\alpha \nabla \cdot \mathbf{u}_{\alpha t}] - \mu^2 [\nabla z_{\alpha t} \nabla \cdot (h \mathbf{u}_\alpha) + \nabla (z_\alpha z_{\alpha t}) \nabla \cdot \mathbf{u}_\alpha] \quad (11)$$

Again, the last set of terms is new.

From here, the mass conservation equation remains Eq. (4), but with

$$\mathbf{M} = (h + \delta\eta) \left\{ \mu_\alpha^2 + \mu^2 \left[ \frac{1}{2} z_\alpha - \frac{1}{6} (h^2 - h\delta\eta + (\delta\eta)^2) \right] \nabla(\nabla \cdot \mathbf{u}_\alpha) + \mu^2 \left[ z_\alpha + \frac{1}{2} (h - \delta\eta) \right] \nabla[\nabla \cdot (h\mathbf{u}_\alpha)] \right\} \quad (12)$$

which is identical to WKGS. The equations for conservation of momentum become

$$\mathbf{u}_{\alpha t} + \delta(\mathbf{u}_\alpha \cdot \nabla)\mathbf{u}_\alpha + \nabla\eta + \mu^2 \mathbf{V}_1 + \delta\mu^2 \mathbf{V}_2 = 0 \quad (13)$$

where

$$\begin{aligned} \mathbf{V}_1 &= \left[ \frac{1}{2} z_\alpha^2 \nabla(\nabla \cdot \mathbf{u}_\alpha) + z_\alpha \nabla[\nabla \cdot (h\mathbf{u}_\alpha)] \right]_t - \nabla \left[ \frac{1}{2} (\delta\eta)^2 \nabla \cdot \mathbf{u}_{\alpha t} + \delta\eta \nabla \cdot (h\mathbf{u}_{\alpha t}) \right], \\ \mathbf{V}_2 &= \nabla \left\{ (z_\alpha - \delta\eta)(\mathbf{u}_\alpha \cdot \nabla)[\nabla \cdot (h\mathbf{u}_\alpha)] + \frac{1}{2} (z_\alpha^2 - (\delta\eta)^2)(\mathbf{u}_\alpha \cdot \nabla)(\nabla \cdot \mathbf{u}_\alpha) \right\} + \frac{1}{2} \nabla \{ [\nabla \cdot (h\mathbf{u}_\alpha) + \delta\eta \nabla \cdot \mathbf{u}_\alpha]^2 \} \end{aligned} \quad (14)$$

The only difference from the original WKGS equations is in the first part of  $\mathbf{V}_1$ , where the temporal derivative originally found only as  $\mathbf{u}_{\alpha t}$  now encompasses the entire term. This small difference ensures that the additional effort required in coding the new equations ranges from minor to almost trivial, depending on the particulars of the computational scheme used.

The question of the definition of  $z_\alpha$  now arises. In all situations here, it will be assumed that

$$z_\alpha = \zeta h + \beta \delta\eta \quad (15)$$

and thus

$$z_{\alpha t} = \beta \delta\eta_t \quad (16)$$

This is a simple time-varying representation analogous to the definition of  $z_\alpha$  adopted by Nwogu,  $z_\alpha = \zeta h$ . Thus, to recover the WKGS equations, simply set  $\beta = 0$ . The Boussinesq equations derived here thus use the velocity (or velocity potential) at reference elevation  $z_\alpha$ , which moves with the instantaneous free surface.

Essentially, this new representation of  $z_\alpha$  does nonlinearly what Nwogu did linearly: it provides a physically based free parameter that may be chosen to improve asymptotically certain properties of interest, even though the overall equations remain at the same level of approximation. For Nwogu, linear dispersion was improved, while here, second-order nonlinear characteristics will be used to choose a value for the initially free parameter,  $\beta$ .

## 2.2. Datum invariant equations

One special case is worth considering in detail. If the reference elevation is written

$$z_\alpha = -h + \beta(h + \delta\eta) \quad (17)$$

and thus, from Eq. (15),  $\beta = \zeta + 1$  ( $=\sqrt{1/5}$  for Padé [2, 2] dispersion), the reference elevation will always be a fixed fraction of the water column from the bed. This reference elevation will give a set of extended WKGS equations whose properties are independent of the definition of the still water level. Note that this choice would also correspond to using a fixed reference coordinate  $\sigma_\alpha$  in a  $\sigma$ -coordinate system based on the instantaneous free surface location.

With the exception of the fully nonlinear  $(\eta, \bar{\mathbf{u}})$  equations of Kirby [11], (and Mei [10], for constant depth) all sets of Boussinesq-type equations known to the authors have had a dependence on the definition of the still water level for both dispersive and nonlinear effects. A set of equations whose properties are invariant with respect to the zero datum but with improved dispersion could have real advantages in situations where mean water levels change significantly over time, e.g. in strongly tidal regions.

The datum-invariant WKGS equations may be found simply by substituting Eq. (17) into Eqs. (12)–(14). The mass equation remains as

$$\eta_t + \nabla \cdot \mathbf{M} = 0 \tag{18}$$

but with

$$\mathbf{M} = (h + \delta\eta) \left\{ \mathbf{u}_\alpha + \mu^2 \left[ (h + \delta\eta)^2 \frac{1}{2} \left( \beta^2 - \frac{1}{3} \right) \right] \nabla(\nabla \cdot \mathbf{u}_\alpha) + \mu^2 \left( (h + \delta\eta) \left( \beta - \frac{1}{2} \right) \right) [\nabla h(\nabla \cdot \mathbf{u}_\alpha) + \nabla(\mathbf{u}_\alpha \cdot \nabla h)] \right\} \tag{19}$$

The equation for conservation of momentum is

$$\mathbf{u}_{\alpha t} + \delta(\mathbf{u}_\alpha \cdot \nabla)\mathbf{u}_\alpha + \nabla\eta + \mu^2 \mathbf{V}_{1s} + \delta\mu^2 \mathbf{V}_{2s} + \delta\mu^2 \mathbf{V}_{3s} = 0 \tag{20}$$

but with

$$\mathbf{V}_{1s} = \frac{1}{2}(\beta^2 - 1)(h + \delta\eta)^2 \nabla(\nabla \cdot \mathbf{u}_{\alpha t}) + (\beta - 1)(h + \delta\eta) [\nabla h \nabla \cdot \mathbf{u}_{\alpha t} + \nabla(\nabla h \cdot \mathbf{u}_{\alpha t})] - (h + \delta\eta) \nabla \delta\eta \nabla \cdot \mathbf{u}_{\alpha t} - \nabla \delta\eta (\mathbf{u}_{\alpha t} \cdot \nabla h) \tag{21}$$

$$\mathbf{V}_{2s} = \nabla \left[ \frac{1}{2}(\beta^2 - 1)(h + \delta\eta)^2 (\mathbf{u}_\alpha \cdot \nabla)(\nabla \cdot \mathbf{u}_\alpha) + (\beta - 1)(h + \delta\eta) \mathbf{u}_\alpha \cdot [\nabla(\mathbf{u}_\alpha \cdot \nabla h) + \nabla h \nabla \cdot \mathbf{u}_\alpha] \right] + \frac{1}{2} \nabla \{ [(h + \delta\eta) \nabla \cdot \mathbf{u}_\alpha + \mathbf{u}_\alpha \cdot \nabla h]^2 \} \tag{22}$$

$$\mathbf{V}_{3s} = \beta \eta_t [\beta(h + \delta\eta) \nabla(\nabla \cdot \mathbf{u}_\alpha) + \nabla(\mathbf{u}_\alpha \cdot \nabla h) + \nabla h \nabla \cdot \mathbf{u}_\alpha] \tag{23}$$

Although derivatives of  $h$  and  $\eta$  appear separately in the equations, as terms arising from bottom slopes and surface slopes, these are independent of where the still water datum is defined. All other references are to  $h + \delta\eta$  together.

### 3. Stokes-type analysis

Linearly, the modified equations of the previous section are identical to WKGS. Correct wave blocking behaviour on a steady current is also maintained, to the order of approximation. However, because new nonlinear terms appear at  $O(\mu^2)$ , nonlinear characteristics will be different. The details of second-order Stokes-type analysis are well known and can provide a valuable prediction of nonlinear performance for many types of equations. Analysis of second-order characteristics was therefore used in order to find the effect of the new free parameter  $\beta$ . Reverting to dimensional form, and restricting the analysis to one horizontal dimension, the independent variables  $\eta$  and  $u_\alpha$  are expanded as

$$\eta = \epsilon \eta_1 + \epsilon^2 \eta_2 + \dots, \quad u_\alpha = \epsilon u_1 + \epsilon^2 u_2 + \dots \tag{24}$$

where  $\epsilon$  here is used as an ordering parameter, which is assumed to be small for the purposes of the Stokes expansion. This is then substituted into Eqs. (12)–(14) to give leading order equations

$$\eta_{1t} + hu_{1x} + h^3 \left( \alpha + \frac{1}{3} \right) u_{1xxx} = 0 \tag{25}$$

$$u_{1t} + g\eta_{1x} + h^2 \alpha u_{1xt} = 0 \tag{26}$$

and at  $O(\epsilon^2)$

$$\eta_{2t} + hu_{2x} + h^3 \left( \alpha + \frac{1}{3} \right) u_{2xxx} = -[\eta_1 u_1]_x - h^2 (\alpha + \gamma) [\eta_1 u_{1xx}]_x \tag{27}$$

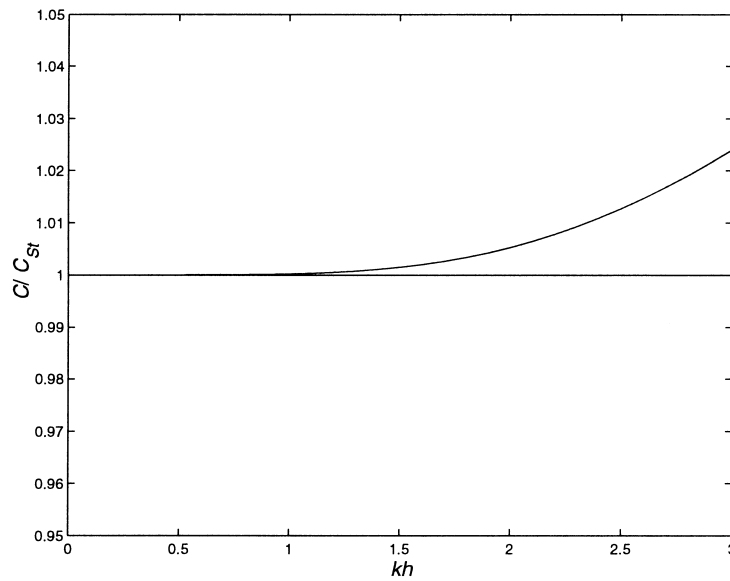


Fig. 1. Boussinesq linear phase speed relative to full linear solution.

$$u_{2t} + g\eta_{2x} + h^2\alpha u_{2xxt} = -\frac{1}{2}[u_1^2]_x + h[\eta_1 u_{1xt}]_x - h^2\alpha[u_1 u_{1xx}]_x - \frac{1}{2}h^2[u_{1x}^2]_x - h\gamma[\eta_1 u_{1xx}]_t \quad (28)$$

where  $\alpha = \zeta^2/2 + \zeta$ , and  $\gamma = \beta(1 + \zeta)$ .

### 3.1. Steady waves

Comparison of solutions for a second-order steady wave with the full second-order Stokes solution provides a way to specify the value of the free parameter  $\gamma$ . For a wave travelling in the positive  $x$ -direction with wave number  $k$  and amplitude  $a_1$ , the first-order solution to Eqs. (25) and (26) is

$$\eta_1 = a_1 \cos(kx - \omega t + \varphi) \quad (29)$$

$$u_1 = a_1 T_{r1} \cos(kx - \omega t + \varphi) \quad (30)$$

where

$$\omega^2 = gk^2 h \frac{1 - (\alpha + (1/3))(kh)^2}{1 - \alpha(kh)^2} \quad (31)$$

$$T_{r1} = \frac{\omega}{kh} \frac{1}{1 - (\alpha + (1/3))(kh)^2} \quad (32)$$

This is the normal linear solution for a steady wave, and is unchanged from WKGS and Nwogu. If the free coefficient is set to  $\alpha = -2/5$ , the resulting phase speed becomes a Padé [2, 2] approximant to the linear Stokes solution. Using this value, Fig. 1 shows the ratio of the phase speed  $\omega/k$  to the linear Stokes phase speed  $c_{St}/\sqrt{gh} = \sqrt{\tanh(kh)/kh}$  over the range  $0 \leq kh < 3$ . Agreement is good over the entire range, but it is clear that  $kh = 3$  is at the limit of linear capabilities, as is well known.

The first-order solution provides forcing to the second-order solutions on the right hand sides of Eqs. (27) and (28). The second-order bound wave then has the form

$$\eta_2 = a_2 \cos(2(kx - \omega t + \varphi)) \quad (33)$$

$$u_2 = u_2 \cos(2(kx - \omega t + \varphi)) \quad (34)$$

The coefficients  $a_2$  and  $u_2$  are given by

$$a_2 = \frac{m_{22}b_{11} - m_{12}b_{22}}{m_{11}m_{22} - m_{12}m_{21}}, \quad u_2 = \frac{m_{11}b_{22} - m_{21}b_{11}}{m_{11}m_{22} - m_{12}m_{21}} \quad (35)$$

where

$$m_{11} = 2\omega, \quad m_{12} = -2kh \left(1 - 4(kh)^2 \left(\alpha + \frac{1}{3}\right)\right), \quad m_{21} = -2gk, \quad m_{22} = 2\omega(1 - 4\alpha(kh)^2) \quad (36)$$

and

$$b_{11} = \frac{a_1^2}{h} kh T_{r1} [1 - (\alpha + \gamma)(kh)^2], \quad b_{22} = \frac{a_1^2}{h} kh T_{r1} \left[ \frac{T_{r1}}{2} + \omega(kh)(\gamma - 1) - (kh)^2 T_{r1} \left(\frac{1}{2} + \alpha\right) \right] \quad (37)$$

The second-order component of the surface elevation may be compared to the full Stokes second-order solution,

$$a_{2St} = \frac{1}{4} \frac{a_1^2}{h} kh \coth(kh) (3 \coth^2(kh) - 1) \quad (38)$$

Following Madsen and Schäffer [5], Eq. (38) may be expanded about  $kh = 0$  to yield

$$a_{2St} = \frac{3}{4} \frac{a_1^2}{h} \frac{1}{(kh)^2} \left( 1 + \frac{2}{3}(kh)^2 + \frac{7}{45}(kh)^4 + O((kh)^6) \right) \quad (39)$$

The Boussinesq solution,  $a_2$ , may be expanded in the same manner. For the extended WKGS equations using  $\alpha = -2/5$ , the corresponding expansion is

$$a_2 = \frac{3}{4} \frac{a_1^2}{h} \frac{1}{(kh)^2} \left( 1 + \frac{2}{3}(kh)^2 + \left( \frac{52}{225} - \frac{8}{9}\gamma \right) (kh)^4 + O((kh)^6) \right) \quad (40)$$

Thus, using  $\alpha = -2/5$ , the value of the coefficient at  $(kh)^2$  is identical to that given from the full Stokes expansion no matter what the value of the free nonlinearity parameter  $\gamma$ . To match the coefficient at  $(kh)^4$  to the exact value of  $7/45$ , however, the free parameter,  $\gamma$ , must be set to

$$\gamma = \frac{17}{200} \quad (41)$$

For the purposes of this paper Eq. (41) will be referred to as the “optimal set”. For the original WKGS equations ( $\gamma = 0$ ) and the datum invariant equations ( $\gamma = 1/5$ ), the coefficient at  $(kh)^4$  will not be matched, and thus nonlinear performance may be expected to suffer somewhat in comparison. Obviously, matching one more coefficient for a second-order steady wave does not necessarily guarantee that overall nonlinear performance will improve. However, when comparing practical computational performance, overall nonlinear accuracy improves considerably, as will be shown.

### 3.2. Superharmonic and subharmonic interactions

For a more realistic sea state composed of waves with varying wavenumbers, frequencies, and amplitudes, the second-order interactions are somewhat more complex. This is most easily illustrated for a simple system with only two first-order components,

$$\eta_1 = a_{1,1} \cos(\psi_1) + a_{1,2} \cos(\psi_2), \quad (42)$$

$$u_1 = a_{1,1} T_{r1} \cos(\psi_1) + a_{1,2} T_{r2} \cos(\psi_2) \quad (43)$$

where  $\psi_1 = k_1x - \omega_1t + \varphi_1$ ,  $\psi_2 = k_2x - \omega_2t + \varphi_2$ , and  $T_{r1}$ ,  $T_{r2}$  satisfy Eq. (32).

The second-order forced waves will be

$$\eta_2 = a_{2,11} \cos(2\psi_1) + a_{2,22} \cos(2\psi_2) + a_+ \cos(\psi_1 + \psi_2) + a_- \cos(\psi_1 - \psi_2) \quad (44)$$

$$u_2 = u_{2,11} \cos(2\psi_1) + u_{2,22} \cos(2\psi_2) + u_+ \cos(\psi_1 + \psi_2) + u_- \cos(\psi_1 - \psi_2) \quad (45)$$

The amplitudes  $a_{2,11}$ , etc., are simply the forced second harmonics of the previous section, but  $a_+$ ,  $a_-$ , etc., give components at the sum and difference of the two frequencies. Defining  $k_{\pm} = k_1 \pm k_2$ ,  $\omega_{\pm} = \omega_1 \pm \omega_2$ , the sum and difference amplitudes,  $a_{\pm}$ ,  $u_{\pm}$  are

$$a_{\pm} = \frac{m_{22\pm}b_{11\pm} - m_{12\pm}b_{22\pm}}{m_{11\pm}m_{22\pm} - m_{12\pm}m_{21\pm}}, \quad u_{\pm} = \frac{m_{11\pm}b_{22\pm} - m_{21\pm}b_{11\pm}}{m_{11\pm}m_{22\pm} - m_{12\pm}m_{21\pm}} \quad (46)$$

where

$$m_{1,1,\pm} = \omega_{\pm}, \quad m_{1,2,\pm} = -k_{\pm}h \left(1 - \left(\alpha + \frac{1}{3}\right)(k_{\pm}h)^2\right), \quad (47)$$

$$m_{2,1,\pm} = -gk_{\pm}h, \quad m_{2,2,\pm} = \omega_{\pm}(1 - \alpha(k_{\pm}h)^2) \quad (48)$$

$$b_{11\pm} = \frac{1}{2}(a_{1,1}a_{1,2})k_{\pm}[(T_{r1} + T_{r2}) - (\alpha + \gamma)(T_{r1}(k_1h)^2 + T_{r2}(k_2h)^2)] \quad (48)$$

$$b_{22\pm} = \frac{1}{2}a_{1,1}a_{1,2}\{k_{\pm}[T_{r1}T_{r2}(1 - \alpha((k_1h)^2 + (k_2h)^2) \mp (k_1h)(k_2h)) - (T_{r1}\omega_1k_1h + T_{r2}\omega_2k_2h)] \\ + \omega_{\pm}\gamma(T_{r1}k_1hk_1 + T_{r2}k_2hk_2)\} \quad (49)$$

These approximate values may now be compared with exact expressions given by Dean and Sharma [12]. Three variants will be compared: the original WKGS equations, the datum invariant equations of Section 2.2, and the “optimal set” (Eq. (41)), which was chosen by comparison with steady waves. All results shown will use  $\alpha = -2/5$ , which results in a [2, 2] Padé approximant to the dispersion relationship.

To begin, results will be shown for all three models as the wavenumbers coalesce, i.e.  $k_1 \Rightarrow k_2$ . For superharmonics, this gives results equivalent to the second harmonic of a steady wave, as in the previous section, while subharmonics correspond to setdown under a wave group. Fig. 2 shows the superharmonics and subharmonics relative to the exact solution. For superharmonics, the WKGS equations show little error for small wavenumbers, but in deeper water, the magnitude of the second harmonic is overpredicted considerably. The datum invariant WKGS equations show a similar magnitude of error, but with amplitudes underpredicted somewhat in intermediate depths. This may have some computational advantages with respect to stability. The optimal set, as expected, shows very good accuracy for the entire range, giving hope that computational results for problems such as nonlinear shoaling may also be improved.

In contrast to the superharmonics, all three sets of equations show identical subharmonic (setdown) performance for  $k_1 \Rightarrow k_2$ . Magnitudes are reasonable until a depth of about  $kh = 1.5$ , when accuracy decreases quickly. Fortunately, wave induced setdown is most important in this shallow region where the model has good accuracy. The reason for identical setdown may be easily seen if the analysis is performed in  $(\eta, \phi)$  space, where the temporal derivatives resulting from the moving reference elevation approach zero as  $k_1 \Rightarrow k_2$ , while other terms remain finite. A similar result was found by Kennedy [13] for a potential flow model when considering time varying and time invariant collocation points.

A more complete understanding of performance may be found by examining Figs. 3–5 which show results for the full superharmonic and subharmonic range relative to full Stokes solutions, for colinear-propagating waves. Amplitudes on the diagonals are identical to the previous figure. The WKGS equations, given in Fig. 3, show superharmonic error increasing steadily with increasing wave number, with more than 30% relative error for dimensionless wave numbers near  $kh = 3$ . Subharmonics, however, show more complicated behaviour. Along the diagonal near the self-interaction line, amplitudes are underpredicted, while the interaction of longer waves with shorter waves near  $k_2h = 0$  shows an overprediction of subharmonic amplitudes.

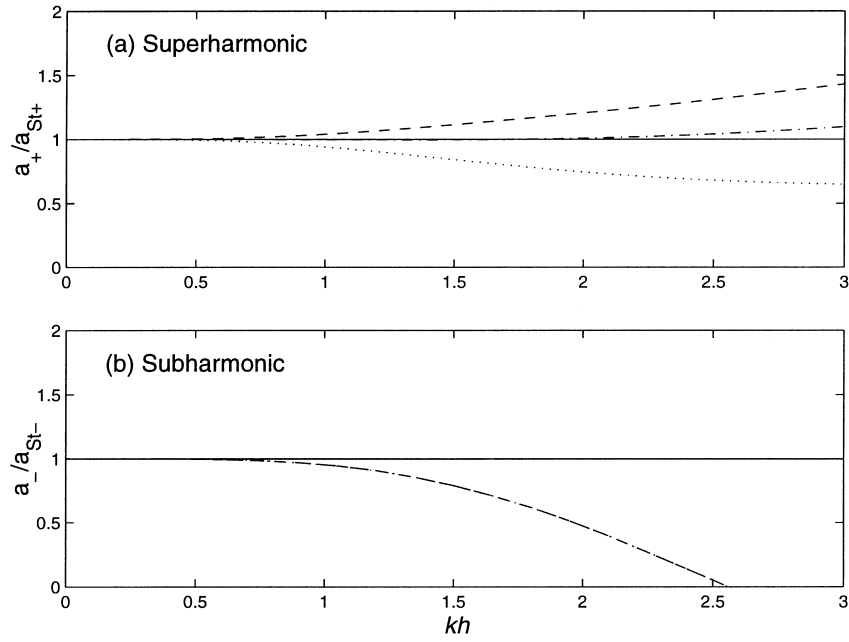


Fig. 2. Self interaction superharmonics (a), and subharmonics (setdown) (b) relative to full Stokes solution. (---) WKGS; (-.-) optimal WKGS; (···) datum invariant WKGS.

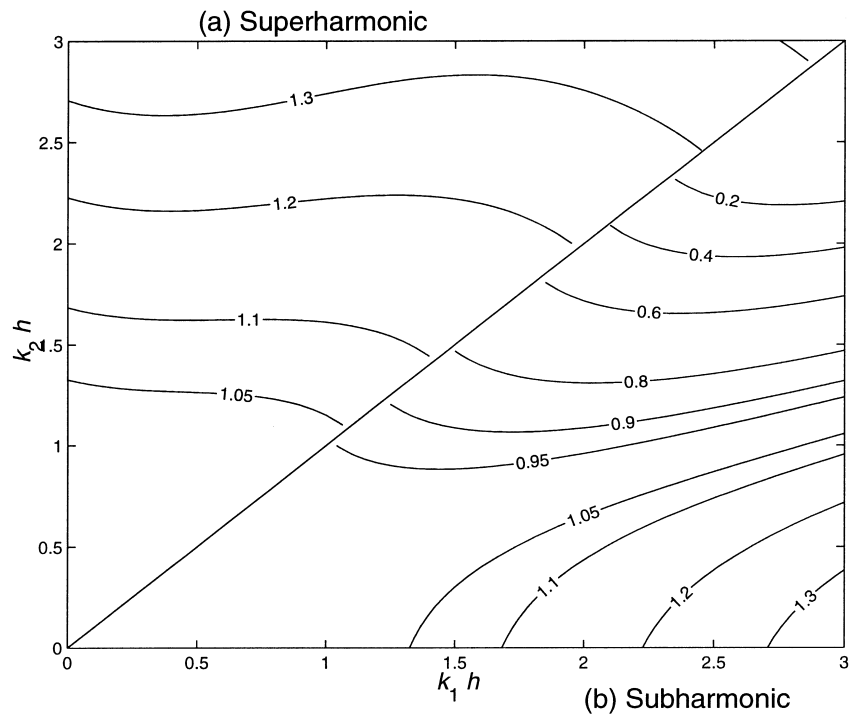


Fig. 3. Second order superharmonic (a) and subharmonic (b) amplitudes for WKGS equations relative to full Stokes solution.

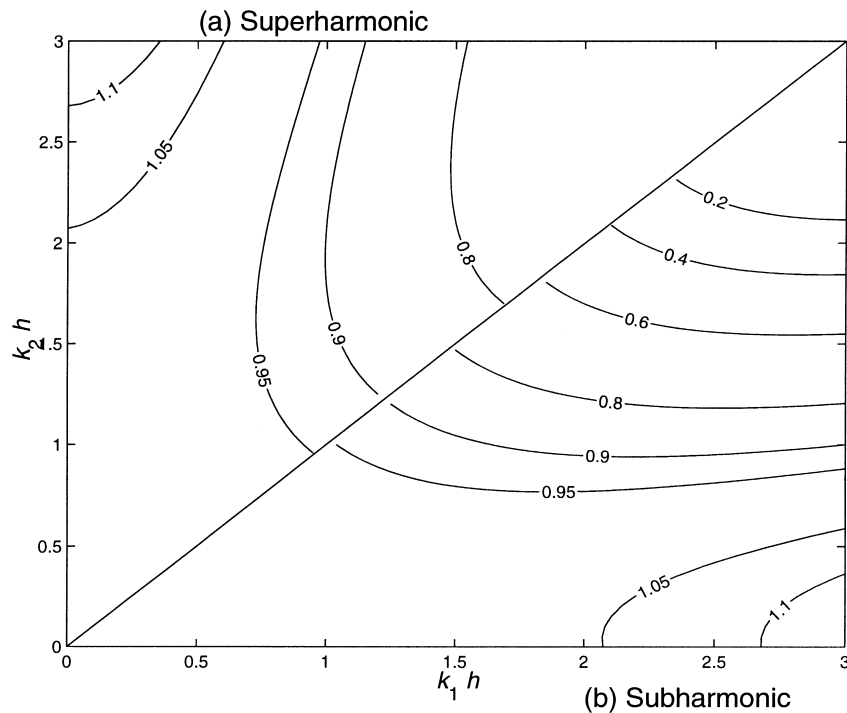


Fig. 4. Second order superharmonic (a) and subharmonic (b) amplitudes for datum invariant WKGS equations relative to full Stokes solution.

Fig. 4 shows the relative amplitudes for the datum invariant WKGS equations, which have a somewhat different pattern. Superharmonic interactions show somewhat underpredicted magnitudes near the diagonal, while away from the diagonal, magnitudes are overpredicted, but by less than the original WKGS equations. Subharmonics show minor differences from the WKGS equations, as might be expected from Fig. 2

Fig. 5 shows results for the optimal WKGS equations. As expected, superharmonic results are best near the self-interaction diagonal, but accuracy is seen to improve everywhere. Subharmonic results, however, once again show relatively small differences from the original WKGS equations. It appears likely that, although the procedure introduced here can significantly improve some measures of nonlinearity and, looking ahead, practical performance, an asymptotic improvement in *all* measures will likely require an  $O(\mu^4)$  model.

Accuracy may be quantified using the index of agreement

$$I_1 = \sqrt{\frac{1}{2(k_{\text{up}}h)^2} \int_0^{k_{\text{up}}h} \int_0^{k_{\text{up}}h} \left( \frac{a_+}{a_{+\text{St}}} - 1 \right)^2 + \left( \frac{a_-}{a_{-\text{St}}} - 1 \right)^2 d(k_1h) d(k_2h)} \quad (50)$$

where  $a_+$  and  $a_-$  are, respectively, the second-order Boussinesq super- and subharmonic transfer functions for surface elevation, and  $a_{+\text{St}}$  and  $a_{-\text{St}}$  are the corresponding full solutions. The upper limit of optimisation was taken to be  $k_{\text{up}}h$  and  $k_1h, k_2h$  are the wavenumber pairs considered. Results were quite similar, although some improvement was found. The original WKGS equations gave a value of  $I_1 = 0.298$ , while, for the datum invariant and optimal WKGS equations, the results were  $I_1 = 0.284$  and  $0.265$ , respectively. The relatively small changes in this quantity were because of the insensitivity of subharmonics to the moving  $z_\alpha$  parameter,  $\gamma$ . Since most of the error was concentrated in the subharmonics, the index  $I_1$  also changed little.

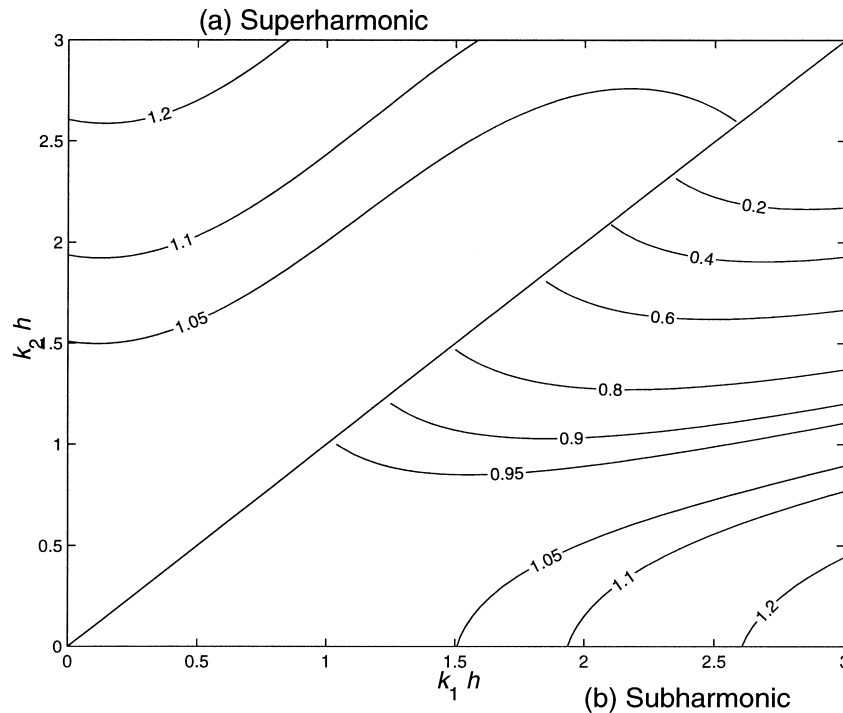


Fig. 5. Second order superharmonic (a) and subharmonic (b) amplitudes for optimal WKGS equations relative to full Stokes solution.

#### 4. Computational tests

With some additional effort, the Stokes-type expansions of the previous section could be extended to higher order, giving information about amplitude dispersion and higher harmonics. However, in a strict sense, even the general usefulness of our second-order analysis may be questioned since Stokes expansions in shallow water converge only for quite small waves. The previous section's manipulation of the error for mildly nonlinear waves is thus not guaranteed to decrease error for highly nonlinear wave transformation in shallow water, something in which we are very interested.

Therefore, to test the utility of the new equations, computational tests were performed. Unsteady shoaling tests were chosen because Boussinesq equations are most often used to compute wave transformation on a sloping beach. To eliminate comparison difficulties that could arise from differing wave generation schemes, all tests were initial value problems, where a specified free surface distribution was allowed to shoal over a given topography. Results were compared to those found using the potential flow model of Kennedy and Fenton [14], which was run using several levels of approximation and discretisation to ensure convergence to the correct solution.

Boussinesq computations used quasi-fourth-order spatial finite difference discretisation, in which first derivatives were computed using fourth-order central differences, but higher derivatives were calculated using second-order differences. At the domain boundaries, symmetry was used to specify exact wall boundary conditions. Time differencing was computed using the fourth-order Runge–Kutta method. No filters were used.

##### 4.1. Unsteady, nonlinear, shoaling waves

All three computational tests simulated wave shoaling, and together covered a wide range of wave heights from near-linear to near-breaking. Normalising all quantities with respect to the greatest depth,  $h_1$ , the topography was

Table 1  
Simulation conditions for unsteady shoaling tests

Case	$a_1/h_1$	$T\sqrt{g/h_1}$
1	0.125	45
2	0.09	70
3	0.075	90

specified as

$$\frac{h}{h_1} = \frac{h_{\min}}{h_1} + \left(1 - \frac{h_{\min}}{h_1}\right) \left[ \frac{1}{\cosh(\tan(\pi x/2L))} \right], \quad x \leq L \quad \frac{h}{h_1} = \frac{h_{\min}}{h_1}, \quad L < x \leq 2L \quad (51)$$

where  $h_{\min}/h_1 = 0.2$ , and  $L = 50h_1$ . Vertical walls were specified at the left and right boundaries. The initial surface elevation was

$$\frac{\eta}{h_1} = \frac{a_1}{h_1} \left[ \frac{\cos(2\pi N_w x/L)}{\cosh(\tan(\pi x/2L))} \right], \quad x \leq L, \quad \frac{\eta}{h_1} = 0, \quad L < x \leq 2L \quad (52)$$

where  $a_1/h_1$  is the initial amplitude, and the number of waves  $N_w = 10$ . All initial velocities were set to zero. The system was allowed to evolve in time until the shoaling waves were quite large.

By varying the initial surface amplitude of the system, somewhat different tests of nonlinear shoaling could be created. Using a large initial amplitude, the first near-breaking waves to appear in the shallow section originated only part of the way down the slope. As the initial amplitude decreased, the first large waves arriving in shallow water originated from increasingly deep water. Computations were stopped when the waves were judged to be near breaking, or had almost all propagated onto the shelf. For the dimensionless wavenumber in the deepest depth,  $kh \approx 1.25$ , linear shoaling characteristics are good through to shallow water [15], so differences from the accurate potential flow model should be almost entirely due to nonlinear properties. Table 1 shows the initial amplitudes,  $a_1/h_1$ , and simulation times,  $T\sqrt{g/h_1}$ , for the three tests.

The output from the tests was examined in several ways, and the points of interest were found to be shown most clearly by considering crest and trough envelopes, the maximum and minimum elevations recorded during the simulations at all points in the domain. These were used to determine wave heights on the slope and shelf, and compared to results from the potential flow model.

Figs. 6–8 show the topography, initial and final surface elevations for cases 1–3, and envelopes from the potential flow model. The initial amplitude was largest in case 1, and thus the simulation could only proceed for a relatively short time until the waves were near breaking. For cases 2 and 3, the initial amplitudes were successively smaller, and the simulation times correspondingly longer. Because of the modulation of the initial surface amplitude, the first waves to propagate onto the shelf were quite small, but were followed by successively larger waves. In the shallower sections, envelopes at any location are thus due to the last wave to pass that point, and the wave fronts may be seen clearly from the apparent discontinuities in the envelope. This gave a range of wave heights for a more complete picture of nonlinear performance. In deeper water, strong modulation of the envelope follows from the partially standing wave system created by the initial conditions. At the finish of computations, cases 1 and 2 had waves that were very large, while waves in case 3 were somewhat smaller, but still highly nonlinear.

In deeper water, where waves were weakly nonlinear, and for small heights in shallow water, Boussinesq envelopes were very similar to each other, and to the potential flow results. However, in the highly nonlinear shoaling zone near the beginning of the shelf, results differed significantly, giving a good comparison of nonlinear shoaling properties. Figs. 9–11 show Boussinesq crest and trough envelopes compared to the potential flow results for cases 1–3 over the range  $40 < x/h_1 < 60$ . All sets of equations estimated trough elevations reasonably well, but results for crest envelopes were not as good. In Fig. 9, which gives results for case 1, the original WKGS equations are seen to overpredict crest elevations greatly when wave heights are large. In contrast, the datum invariant WKGS equations

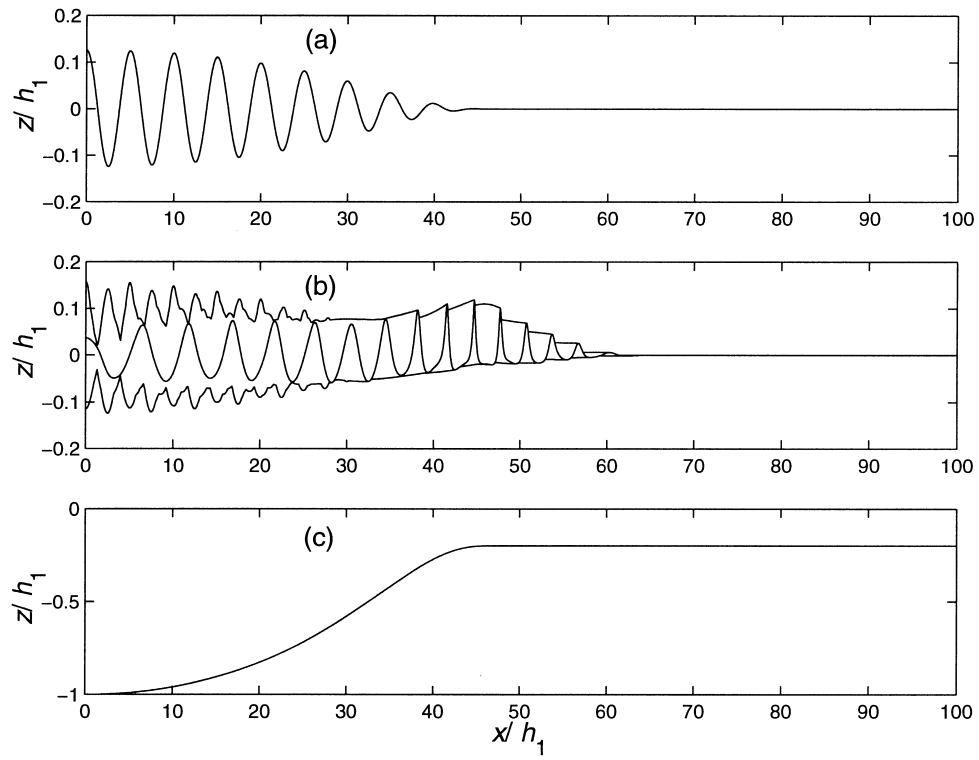


Fig. 6. (a) Initial and (b) final surface elevations for case 1, with crest and trough envelopes; (c) underlying bathymetry.

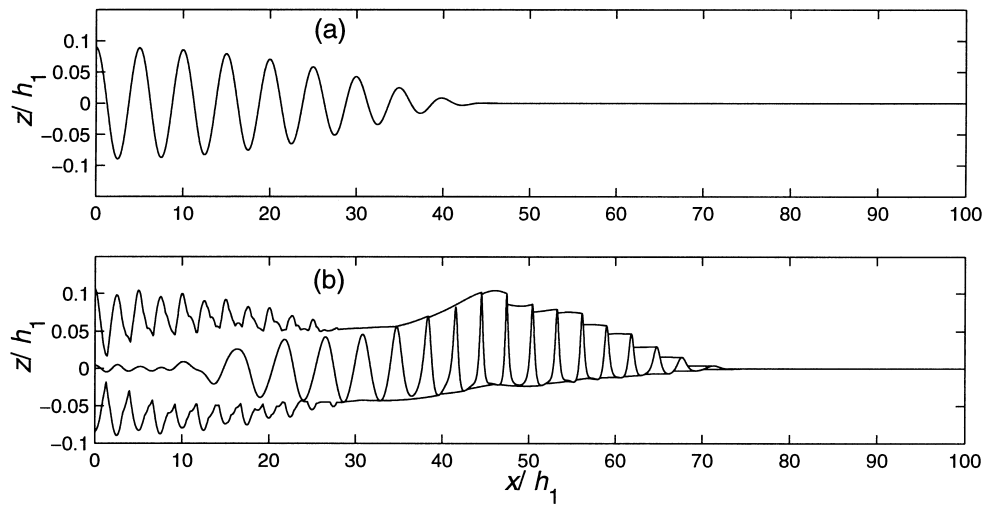


Fig. 7. (a) Initial and (b) final surface elevations for case 2, with crest and trough envelopes.

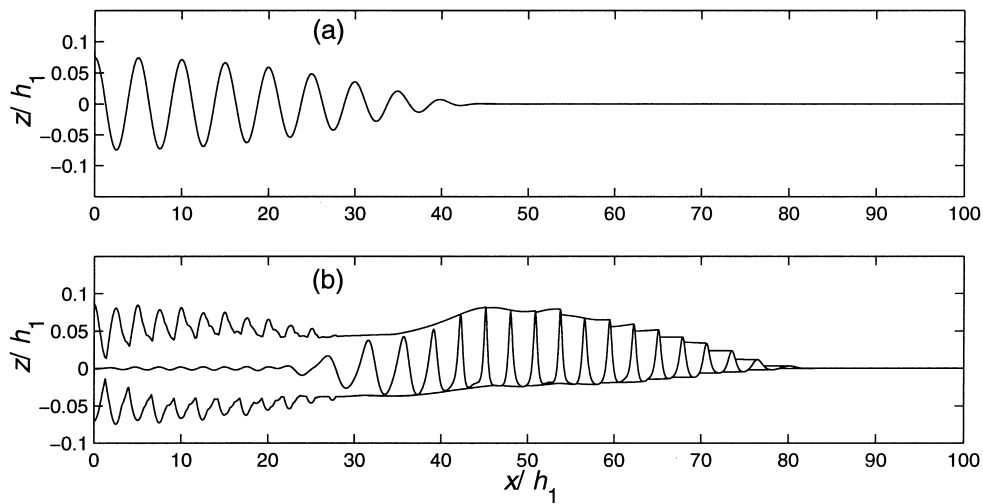


Fig. 8. (a) Initial and (b) final surface elevations for case 3, with crest and trough envelopes.

tend to underpredict crest elevations in this range. However, the optimal set WKGS equations with  $\beta = 17\sqrt{5}/200$ , ( $\gamma = 17/200$ ), provide a very good estimate of crest elevation even for highly nonlinear waves.

An examination of Figs. 10 and 11 shows a similar result. For these tests, the WKGS equations tend to overpredict crest elevations but by far less than was found in test 1. The datum invariant equations tend to underpredict heights, while, once again, the optimal WKGS equations predict crest elevations very well for almost all waves. For all

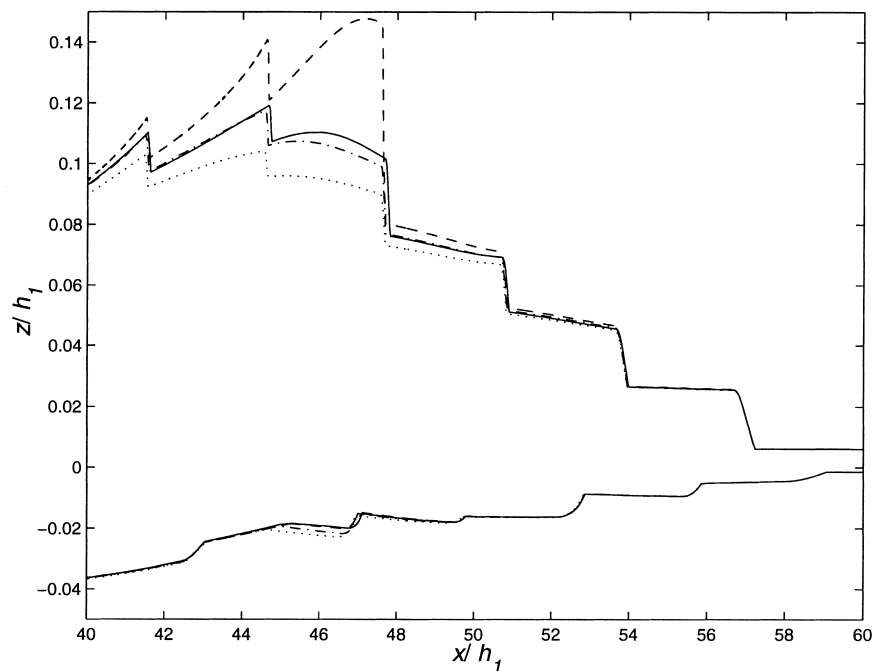


Fig. 9. Crest and trough envelopes for unsteady shoaling, case 1. (—) Accurate potential flow; (---) WKGS; (···) datum invariant WKGS; (-·-) optimal WKGS.

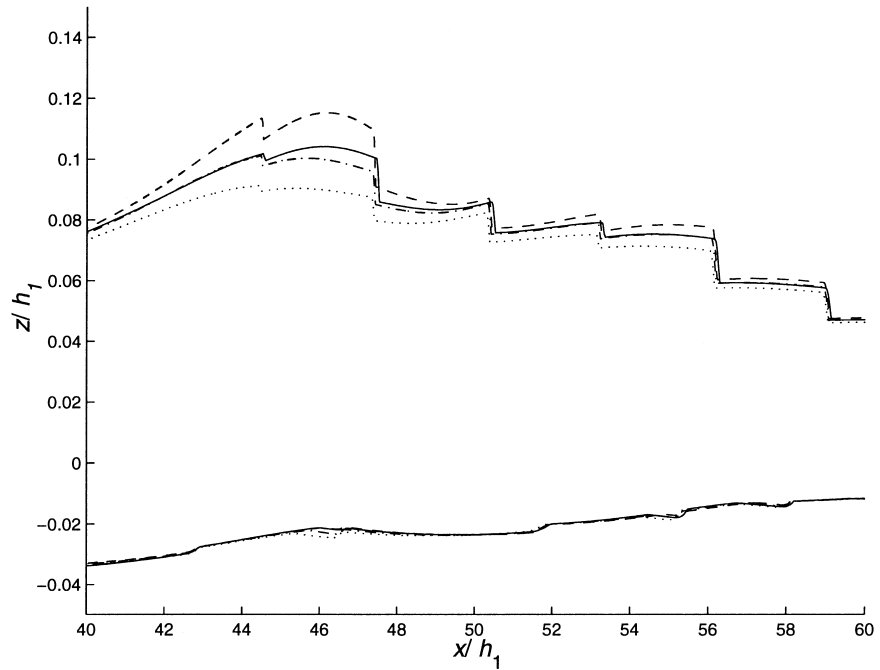


Fig. 10. Crest and trough envelopes for unsteady shoaling, case 2. (—) Accurate potential flow; (---) WKGS; (···) datum invariant WKGS; (-·-) optimal WKGS.

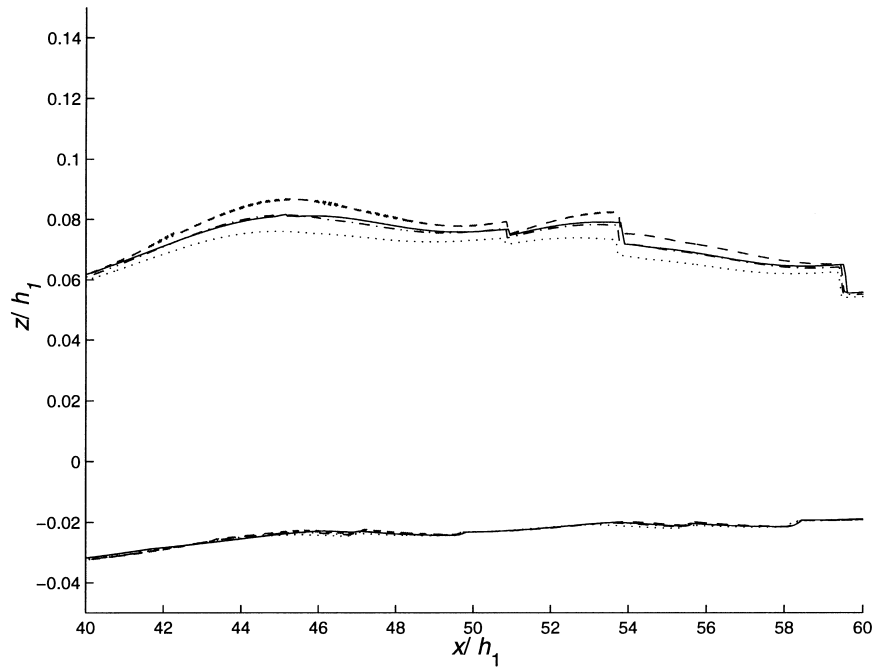


Fig. 11. Crest and trough envelopes for unsteady shoaling, case 3. (—) accurate potential flow; (---) WKGS; (···) datum invariant WKGS; (-·-) optimal WKGS.

equations and all cases, wherever discrepancies exist, they were found to increase strongly with increasing wave height. Thus agreement becomes better for the smaller waves of cases 2 and 3, when compared to case 1. All of these results agree with the trends predicted by second-order superharmonic analysis, even though the Stokes-type expansions used are completely invalid for near breaking shallow water waves. This adds weight to the conjecture given earlier that, for a fully nonlinear system, an increase in asymptotic nonlinearity leads to an overall improvement in finite amplitude nonlinear performance.

One interesting observation is that for large waves all Boussinesq results predict phase speeds that are too small, as seen by the difference in location of the wave envelope fronts. This is in agreement with the results of Otta and Schäffer [16], and WKGS, each of which found all Boussinesq equations tested to underpredict amplitude dispersion, some significantly so. (Note, however, that the degree of underprediction is significantly reduced in models retaining terms to  $O(\mu^4)$ ; see the discussion of solitary wave behaviour in Gobbi et al. [9].)

A secondary result of these tests was that they provided information about the stability and convergence of the various equations, which was found to differ greatly. After repeatedly increasing computational resolution to test for convergence, slowly growing high wavenumber noise was seen after tens of thousands of time steps for some runs with very fine discretisations, even though the Courant number was quite small ( $C_r < 0.1$ ). Although it is difficult to separate the stability of the different equations from the stability of the computational scheme, the most stable set was observed to be the datum invariant WKGS equations, followed by the optimal WKGS, followed by the original WKGS equations. Computational convergence with increasingly finer resolution followed the same path, with the datum invariant equations converging most quickly.

This progression might be expected from an examination of second-order superharmonics, as the datum invariant WKGS equations show lower magnitudes of higher harmonics than the optimal equations and the original WKGS equations. Thus, the datum invariant equations should have less curvature of the free surface, which generally leads to faster convergence and greater stability.

For cases 2 and 3, noise appeared in the original WKGS equations seemingly before convergence had occurred. This has probably led to an underestimate of the crest envelope. All other equations converged before the appearance of any significant noise, although a very small amount was found in results for the optimal set. For case 1, no noise was found in the WKGS equations, but convergence was again not assured. This lack of convergence was found only near  $x/h_1 = 46$ , where the crest of the last wave was very high (Fig. 12). Many successively finer resolutions were tested, but the wave crest became increasingly sharp, and the crest envelope increased correspondingly. As the envelope showed no signs of convergence, indeed, quite the opposite, results are shown for the finest grid spacing tested ( $\Delta x/h_1 = 0.01$ ). A somewhat similar result was obtained in WKGS, where the computed crest elevation of a shoaling solitary wave was found, for gentle slopes, to increase too strongly just before the breaking location.

A different way of examining the data may be seen in Fig. 12. Taking data from the entire domain, and for all three cases, this shows computed local height to depth ratios for accurate potential flow solutions plotted against the same quantity for the Boussinesq results. Wave heights here are computed using crest and trough envelopes. Because the whole domain is used, the scatter plot includes a range of primary wave numbers, from approximately  $0.25 < kh < 1.25$ , and wave heights from  $0 \leq H/h < 0.7$  in various combinations. For the largest wave heights,  $H/h > 0.5$ , wavenumbers are generally in the range  $kh < 0.5$ . The large excursions of a few points below the diagonal from the normal trend of the plot are found at wave fronts. Because wave speeds for Boussinesq and potential flow solutions differed for high waves, as just noted, the exact locations of the wave fronts were also slightly different, causing these anomalies.

For the WKGS equations, wave heights are in good agreement with exact values for small wave heights. However, for  $H/h > 0.5$ , WKGS heights are consistently overpredicted, with this difference increasing steadily with wave height. The datum invariant equations also begin to show some error at around  $H/h = 0.5$ , but instead underpredict wave heights in this highly nonlinear zone. Excepting results at wave fronts, the optimal WKGS equations show significant error only in the range  $H/h > 0.6$ , which is a very good result for an  $O(\mu^2)$  technique.

These results were quantified by computing the root-mean-square error of the crest and trough envelopes when compared to the potential flow solution. Results were normalised using the initial wave amplitude,  $a_1/h_1$ . Since

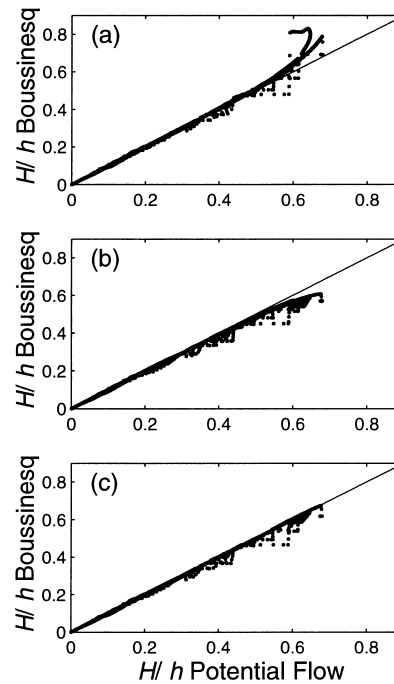


Fig. 12. Height to depth ratios for Boussinesq equations compared to accurate potential flow calculations, cases 1–3 combined: (a) WKGS; (b) datum invariant WKGS; (c) optimal set WKGS.

different portions of the domain showed different behaviour, the overall domain was divided into subdomains, and indices  $d_i$  were computed in each subdomain.

Tables 2–4 shows the indices of agreement for the various cases. In the deeper sections, with  $x/h_1 < 40$ , agreement is very good. In the shallowest region, with  $x/h_1 > 50$ , all equations also gave excellent results, because waves were relatively small and in shallow water. An interesting feature found in all regions was that, with one exception, trough envelopes all showed better agreement than crest envelopes, sometimes remarkably so. It thus appears that, not surprisingly, predicting crest elevations is significantly more difficult than trough elevations.

The most interesting portion of the results comes from the region  $40 < x/h_1 < 50$ . Indices of agreement for crest envelopes are much worse here than in any other region because of the highly nonlinear shoaling waves. The standard WKGS equations showed significant error because of the overprediction of crest heights, while the depth invariant WKGS equations generally showed less discrepancy, because the underprediction of crest elevations

Table 2  
Normalised RMS errors for crest and trough envelopes, case 1

Region	Envelope	WKGS	DI WKGS	Optimal WKGS
0–20	Crest	0.0265	0.0219	0.0226
	Trough	0.0149	0.0126	0.0138
20–40	Crest	0.0127	0.0171	0.0096
	Trough	0.0093	0.0053	0.0077
40–50	Crest	0.1417	0.0817	0.0259
	Trough	0.0034	0.0112	0.0064
50–100	Crest	0.0036	0.0050	0.0031
	Trough	0.0001	0.0005	0.0002

Table 3  
Normalised RMS errors for crest and trough envelopes, case 2

Region	Envelope	WKGS	DI WKGS	Optimal WKGS
0–20	Crest	0.0157	0.0141	0.0141
	Trough	0.0114	0.0103	0.0108
20–40	Crest	0.0088	0.0145	0.0091
	Trough	0.0062	0.0046	0.0055
40–50	Crest	0.0768	0.0970	0.0291
	Trough	0.0040	0.0107	0.0054
50–100	Crest	0.0117	0.0196	0.0087
	Trough	0.0024	0.0021	0.0016

Table 4  
Normalised RMS errors for crest and trough envelopes, case 3

Region	Envelope	WKGS	DI WKGS	Optimal WKGS
0–20	Crest	0.0128	0.0121	0.0118
	Trough	0.0099	0.0091	0.0097
20–40	Crest	0.0077	0.0125	0.0087
	Trough	0.0079	0.0068	0.0075
40–50	Crest	0.0340	0.0561	0.0115
	Trough	0.0081	0.0084	0.0070
50–100	Crest	0.0130	0.0262	0.0105
	Trough	0.0019	0.0033	0.0014

was less severe. The optimal WKGS equations gave by far the best performance in this highly nonlinear region, especially for the near-breaking waves found in case 1. Clearly, the improvement in nonlinearity suggested by the second-order analysis is a good predictor of actual performance.

## 5. Discussion and conclusions

It appears likely that higher order equations may also be improved by considering a time-varying reference elevation. In particular, the  $O(\mu^4)$  equations of Gobbi et al. [9] appear suitable for such an extension, which is now being investigated. Related derivations which also lead to improved shoaling properties are being considered.

The enhanced  $\mathbf{u}_\alpha$  equations of Madsen and Schäffer [5] might appear to benefit from this approach, but after some study, no significant benefits were found. Superharmonics could easily be improved asymptotically for small wavenumbers. However, unlike the improved WKGS equations, superharmonics over the range  $1 < kh < 3$  were found to have worse performance than before and thus the asymptotic improvement could not be recommended.

Although nonlinear characteristics were optimised only at second order, it appears that the improvement in these properties for fully nonlinear Boussinesq systems carries through to higher order, as seen by the excellent results for very large shoaling waves. This gives increased confidence in accuracy when studying and predicting physical wave phenomena in the laboratory and in the field, where exact solutions may not be available for comparison.

In conclusion, the Boussinesq-type equations of Wei et al. [6] have been extended to include a reference velocity level that varies in time. Two special cases of these new equations were studied for their special significance: an “optimal set”, where second-order self-interaction superharmonic properties were asymptotically improved, and a “datum invariant” set, which has no dependence on the definition of the still water level. These were compared analytically and computationally with the original WKGS equations.

The optimal set was found to have much improved second-order superharmonic properties, but subharmonics were affected little. Computational tests of nonlinear shoaling waves showed greatly increased accuracy in crest

elevations, especially for very large waves. This set appears to have large advantages when compared to the WKGS equations and no real disadvantages, but still appears less accurate than  $O(\mu^4)$  equations such as Gobbi et al. [9], Gobbi and Kirby [17], or Madsen and Schäffer [5] Section 3–5.

In contrast, the datum invariant equations were found to underpredict nonlinearity for large waves. However, this underprediction came with the added benefit of excellent stability and convergence when compared with the other two sets of equations tested. Furthermore, the invariance of these equations to the definition of the still water level could make these equations useful in situations where the mean water level changes significantly over time. Overall, it would seem that nonlinear accuracy is also somewhat improved when compared with the original WKGS equations.

## Acknowledgements

This study has been supported by the Office of Naval Research, Base Enhancement Program, through research Grant N00014-97-1-0283.

## References

- [1] D.H. Peregrine, Long waves on a beach, *J. Fluid Mech.* 27 (1967) 815–827.
- [2] P.A. Madsen, R. Murray, O.R. Sørensen, A new form of the Boussinesq equations with improved linear dispersion characteristics. Part 1, *Coastal Eng.* 15 (1991) 371–388.
- [3] P.A. Madsen, O.R. Sørensen, A new form of the Boussinesq equations with improved linear dispersion characteristics. Part 2. A slowly varying bathymetry, *Coastal Eng.* 18 (1992) 183–204.
- [4] O. Nwogu, Alternative form of Boussinesq equations for nearshore wave propagation, *J. Waterway, Port, Coastal and Ocean Eng.* 119 (1993) 618–638.
- [5] P.A. Madsen, H.A. Schäffer, Higher order Boussinesq-type equations for surface gravity waves — derivation and analysis, *Phil. Trans. R. Soc. A* 356 (1998) 1–59.
- [6] G. Wei, J.T. Kirby, S.T. Grilli, R. Subramanya, A fully nonlinear Boussinesq model for surface waves. I. Highly nonlinear, unsteady waves, *J. Fluid Mech.* 294 (1995) 71–92.
- [7] S.B. Yoon, P.L.-F. Liu, Interactions of currents and weakly nonlinear water waves in shallow water, *J. Fluid Mech.* 205 (1995) 397–419.
- [8] Q. Chen, P.A. Madsen, H.A. Schäffer, D.R. Basco, Wave-current interaction based on an enhanced Boussinesq approach, *Coastal Eng.* 33 (1998) 11–39.
- [9] M.F. Gobbi, J.T. Kirby, G. Wei, A fully nonlinear Boussinesq model for surface waves. II. Extension to  $O(\mu^4)$ , *J. Fluid Mech.* 405 (2000) 181–210.
- [10] C.C. Mei, *The Applied Dynamics of Surface Ocean Waves*, World Scientific, Singapore, 1989, 740 pp.
- [11] J.T. Kirby, Nonlinear, dispersive long waves in water of variable depth, in: J.N. Hunt (Ed.), *Gravity Waves in Water of Finite Depth*, 1997, pp. 55–125.
- [12] R.G. Dean, J.N. Sharma, Simulation of wave systems due to nonlinear directional spectra, in: *Proceedings of the International Symposium on Hydrodynamics Ocean Eng.*, Trondheim, 1981, pp. 1211–1222.
- [13] A.B. Kennedy, Recent extensions to local polynomial approximation models, in: B.L. Edge (Ed.), *Proceedings of the 26th International Conference on Coastal Eng.*, Copenhagen, 1998, pp. 589–602.
- [14] A.B. Kennedy, J.D. Fenton, A fully-nonlinear computational method for wave propagation over topography, *Coastal Eng.* 32 (1997) 137–161.
- [15] H.A. Schäffer, P.A. Madsen, Discussion of A formal derivation and numerical modelling of the improved Boussinesq equations for varying depth, *Ocean Eng.* 25 (6) (1998) 497–500.
- [16] A.K. Otta, H.A. Schäffer, Finite-amplitude analysis of some Boussinesq-type equations, *Coastal Eng.* 36 (1999) 323–342.
- [17] M.F. Gobbi, J.T. Kirby, Wave evolution over submerged sills: Tests of a high-order Boussinesq model, *Coastal Eng.* 37 (1999) 57–96.